analytical chemistry

pubs.acs.org/ac Article

Membrane Feature-Inspired Profiling of Extracellular Vesicles for Pancreatic Cancer Diagnosis

Ping Li, Jie Wang, Mengqiu Gao, Jue Wang, Yi Ma,* and Yueqing Gu*

Cite This: *Anal. Chem.* 2021, 93, 9860−9868 Read Online

ABSTRACT: Extracellular vesicles (EVs) have recently emerged as a promising tumor biomarker, and EV phenotyping offers many benefits for cancer diagnosis. However, the practicality of EV assays remains a challenge due to macromolecule disturbances, biomarker heterogeneities, and EV abundance limitations. Here, we demonstrate a membrane-based biosensor for precise and sensitive EV identification. The sensor synergistically integrates EV capture and detection by virtue of EV membrane features (membrane protein and lipid bilayer), comprising antibody-conjugated magnetic beads (AbMBs) and duplex-specific nuclease (DSN)-mediated amplification cycles. Bivalent cholesterol (biChol)-modified RNA−DNA duplexes are designed to insert into the EV membrane, transforming EV signals into RNA signals and initiating the signal amplification. The membrane-based signal production pattern eliminates protein interference. By employing four antibodies specific to PCa-related membrane proteins, the AbMB−biChol platform enables the successful differentiation and monitoring of PCa-related EVs and distinguishes PCa patients from healthy donors with improved efficacy, exhibiting superior efficiency over the analyses based on clinically used biomarker CA19-9 and PCa-related proteins. As such, the developed system has great potential for clinical PCa diagnosis.

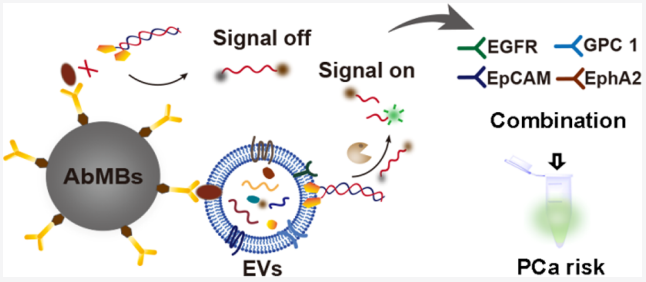

Pancreatic cancer (PCa) is predicted to be the second leading cause of cancer-related deaths within the next 10 years owing to untimely diagnosis and poor prognosis.[1] Currently, carbohydrate antigen 19-9 (CA19-9) is a well-established and noninvasive indicator in routine clinical use. However, serum CA19-9 as an individual marker can be considerably limited for PCa discrimination, resulting in low PCa diagnosis efficacy.[2] Promising PCa diagnostic patterns with effectual or multivariate biomarker analysis have expanded prospective clinical applications.

Recently, studies on extracellular vesicle (EV)-based biomarkers have made headway in cancer diagnosis. EVs are abundantly secreted by most cells and ultimately accumulate in the circulation, which are generic nanoscale particles and delimited by the lipid bilayer naturally.[3] EVs have been favored in biomarker development due to their structural stability, wide distribution, and more importantly, the abundance of multiple biomarkers (proteins, nucleic acids, and lipids).[4−7] To date, EV-based proteomic markers have attracted much attention since their origin and relationship with living cells are better than those of most free serum proteins.[8−11] Typically, by characterizing PCa-related proteins on the membrane of EVs, studies have demonstrated the feasibility of PCa detection and metastatic forecasting.[12−14] Thus, the accurate differentiation of EVs with cancer signatures is regarded as highly beneficial for PCa diagnosis.

While growing evidence has suggested that EV identification reflects cancer states, the current clinical practice of EVs is still challenging since the conventional isolation processes (e.g., ultracentrifugation, ultrafiltration, microfluid-based enrichment, polymer-based precipitation, and cohesion) are nonspecific, complex, and inefficient with long turnaround times.[15−17] Recently, methods have been developed to isolate and identify tumor-derived EVs via specific antibodies binding to the candidate tumor-regulated markers on the EV membrane.[18−20] Nevertheless, such immune affinity-based strategies are inevitably affected by con-specific free proteins, which render the quantification of targeting EV subpopulations inaccurate and compromise sensitivity and specificity. Some studies have utilized different capture ligands (e.g., CD63 and CD81 antibodies) and specific detection ligands simultaneously for precise EV detection, partially abating non-EV signals.[21,22] However, circulating EVs have highly heterogeneous molecular signatures (e.g., lack of capture receptor expression), resulting in the missed detection of specific EVs.

Received: April 22, 2021
Accepted: June 30, 2021
Published: July 12, 2021

https://doi.org/10.1021/acs.analchem.1c01712
Anal. Chem. 2021, 93, 9860−9868

For instance, the CD63 expression of EVs varies greatly in different samples with low abundance observed in plasma, leading to insufficient EV capture efficacy from plasma samples.[23] Furthermore, EV quantification approaches based on membrane proteins result in inaccuracies that arise from variations in target protein abundance on the EV membrane.[24]

Inspired by the features of the lipid bilayer of EVs, we develop a novel EV assay utilizing cholesterol as a hydrophobic moiety that inserts into the EV membrane.[25−27] This lipid affinity-based EV characterization strategy assists signal transformation and eliminates the interference of proteins, precisely reflecting the EV content by accurately quantifying the lipid levels.[28,29] The proposed platform paves the way for the implementation of precise and sensitive EV differentiation and noninvasive PCa detection. In detail, specific antibody-conjugated magnetic beads (AbMBs) and bivalent cholesterol (biChol, cholesterol modified on the adjacent end of each signal strand)-modified RNA−DNA duplexes served as the EV capturer and the signal transporter, respectively. Samples were first incubated with AbMBs and the biChol-modified duplex was anchored on the EV membrane. Then the AbMBs, EVs, and duplexes were isolated by magnetism. Duplex-specific nuclease (DSN), a unique nuclease that is preferable to cleave DNA in RNA−DNA duplexes and is practically inactive toward RNA,[30,31] was introduced for signal amplification. The fluorescent signal emerged and amplified after selective digestion of the DNA probe, followed by recurrent RNA detection cycles. Such amplification cycles produced enhanced fluorescent signals to a great extent for identification (Scheme 1). Modified with antibodies specific to four PCa-related protein biomarkers (EGFR, EpCAM, GPC1, and EphA2), the AbMB−biChol platform exhibited great EV differentiation potential and achieved impressive diagnostic efficacy in discriminating between PCa patients and healthy donors, surpassing clinical biomarker CA19-9 and PCa-related protein analysis.

Scheme 1. Schematic Overview of the AbMB−biChol Platform for Specific EV Detection in Plasma[a]

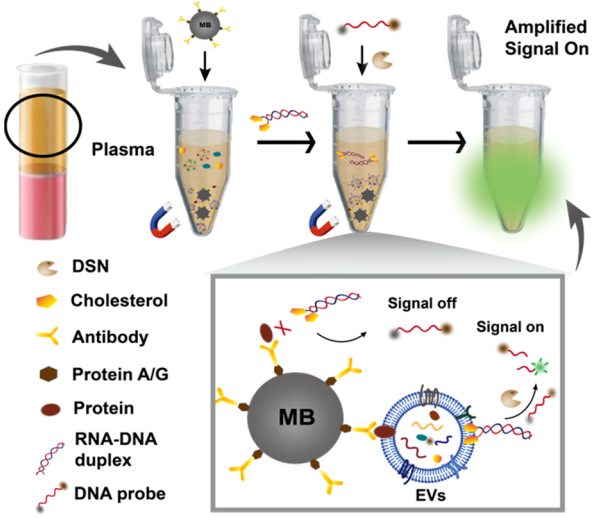

[a]Plasma was collected and incubated with antibody-modified magnetic beads and separated by magnetism. To specifically amplify the EV signal, a cholesterol-modified RNA−DNA duplex was introduced on the EV membrane and the DSN-assisted amplification cycle was initiated, producing an amplified signal, while proteins were unable to trigger the signal for incompatibility with cholesterol.

EXPERIMENTAL SECTION

Reagents and Materials. Protein A/G-modified magnetic beads were purchased from Invitrogen (Dynabeads TM). Antibodies for immune capture or western blot were purchased from Abcam. High-glucose Dulbecco's modified Eagle's medium (DMEM) medium, RPMI-1640, and antibiotics were bought from KeyGEN BioTECH, China. Fetal bovine serum (FBS) was bought from Gibco. Carcinoma cell lines PANC-1, BxPC-3, MCF-7, U87, and THP-1 were purchased from China Type Culture Collection. All of the oligonucleotides used in this work were synthesized by Sangon Biotech, China. The cholesterol-modified duplex and the siRNA-Mate transfection agent were purchased from GenePharma, China. The Trizol Plus RNA purification kit was purchased from Life Technologies. Duplex-specific nuclease (DSN) was purchased from Evrogen, Russia. The poly-A cDNA synthesis kit, SYBR qPCR master kit, and AceTaq master mix kit were purchased from Vazyme, China. The cell-free nucleic extraction kit was purchased from Tiangen, China. The total protein extraction kit, sodium dodecyl sulfate-polyacrylamide gel electrophoresis (SDS-PAGE) preparation kit, and protein quantification kit (BCA method) were purchased from KeyGEN BioTECH, China. Enzyme-linked immunosorbent assay (ELISA) kits (EGFR, EpCAM, GPC1, and EphA2) were purchased from Jianglai Biology, China.

Instrumentation. A NanoDrop One (Thermo Scientific) was employed to determine the UV absorbance of the antibody. A DynaMag-Spin scaffold (Invitrogen) was employed to perform magnetic separation. An Ultracentrifuge (L-80XP, Beckman) was used for EV preseparation. NanoSight NTA system (Malvern, U.K.) was employed for EV quantification and diameter measurement. A real-time polymerase chain reaction (PCR) system (7300Plus, Applied Biosystem) was used for RNA and DNA quantified detection. A fluorescence microscope (DMi8, Leica, Germany) was used for EV observation. A fluorescence spectrophotometer (Hitachi, Japan) was employed for fluorescence signal determination. An Attana Cell 200 (Sweden) was employed for affinity verification between the cholesterol-modified duplex and the cell membrane.

Preparation of Antibody-Modified Magnetic Beads. Dynabeads were preblocked by 5% BSA to reduce the nonspecific binding. Then, the beads were washed with TBST and separated by magnetism 3 times. Twenty microliters of resuspended beads were incubated with 1, 2, 4, 5, and 10 μg of the primary antibody (or IgG) on a rocker platform, separately, and the incubation time was set from 0.5 to 4 h. Then, the antibody amount from the supernatant and beads was detected by electrophoresis and Coomassie blue staining. The UV absorbance at 280 nm of the supernatant was detected for the quantification of the uncombined antibody. The indirect method based on the random RNA (R-RNA) recovery rate was used to confirm the optimized incubation conditions.

Cell Culture and EV Collection by Ultracentrifugation. Fetal calf serum (FBS) was centrifuged first at 120 000g and 4 °C overnight to remove EVs. PANC-1, MCF-7, and U87 cells were cultured in DMEM medium, and BxPC-3 and THP-1 cells were grown in RPMI-1640 medium. All cells were cultured in media supplemented with 10% EV-free FBS, penicillin (100 μg/mL), and streptomycin (100 μg/mL) and

https://doi.org/10.1021/acs.analchem.1c01712
Anal. Chem. 2021, 93, 9860−9868

then maintained in an incubator with 5% CO_2 at 37 °C. The supernatant was collected after being incubated for 48 h. About 100 mL of the supernatant was centrifuged at 300*g* for 10 min, 2000*g* for 20 min, and 10 000*g* for 30 min, to remove cells, cellular debris, and large extracellular vesicles, sequentially.[32] The sediment was collected for EV identification experiments. The concentrations of EVs were detected by NTA.

Clinical Sample Collection. According to the experimental implementation plan and the norms and reasonable operating procedures of collection, the whole process strictly followed the relevant ethical requirements and all volunteers signed the informed consents before collecting the human plasma sample from each of 21 PCa patients and 29 noncancer donors (Table S1). All of the sample donors were fasting for at least 12 h. Ten milliliters of blood samples were collected with ethylenediaminetetraacetic acid (EDTA) anticoagulant tubes and centrifuged at 4 °C for 5 min at 2000*g* to remove blood cells. Then, plasma samples were further centrifuged at 4 °C for 30 min at 20 000*g* to remove cell debris. Plasma samples were then stored at −80°C until further use. Plasma EVs were collected both by the AbMB−biChol platform and the ultracentrifugation platform for practicability verification and comparison of the proposed method, respectively.

R-RNA Transfection, Extraction, and RT-PCR. Random RNA with the sequence (Table S2) was transfected into cells via the siRNA-Mate transfection agent according to the protocol. Then, the cells were further cultured and EVs were collected. Total RNA was extracted from the EVs using the Trizol Plus RNA purification kit. As the random RNA was designed as a short RNA single strand for higher EV loading efficiency, reverse transcription (RT)-PCR by the poly-A method was conducted for R-RNA quantification by the following method: 10 μL of 2 × miRNA solution, 2 μL of the miRNA RT enzyme mix, total RNA extracted from real samples, and DEPC-treated water were mixed to a final volume of 20 μL. The RT process was conducted under the following conditions: 37 min at 60 °C and 5 min at 85 °C. The qRT-PCR process was conducted by the following method: 5 μL of the 2 × SYBR qPCR master mix, 0.2 μL of the forward primer (10 μM), 0.2 μL of the universal reverse primer (10 μM), 2 μL of the RT product, and DEPC-treated water were mixed to a final volume of 10 μL. The qRT-PCR process was conducted under the following conditions: 95 °C for 5 min, 40 cycles of 95 °C for 10 s, and 60 °C for 30 s. The fluorescence signal was detected at 60 °C.

Isolation and Detection of EVs by the AbMB−biChol Platform. Twenty microliters of antibody-modified magnetic beads were collected and incubated with EVs for different times and temperatures and then separated via magnetism. The capture yield was calculated by comparing the R-RNA copies in total EVs and separated EVs, which could be calculated by the following equation[33]

$$\text{EV capture rate} = \frac{\text{R} - \text{RNA transcripts}_{\text{cap}-\text{EV}}}{\text{R} - \text{RNA transcripts}_{\text{total}-\text{EV}}}$$

Different incubation orders were also explored. The separated AbMBs and captured EVs were then incubated with 10 μL of the EV membrane dye PHK 67 and observed under a fluorescence microscope. The cholesterol-modified RNA−DNA duplex (biChol, 1 μM) as well as ribonucleoside vanadyl complexes (RVC, RNA stabilizer) was added and incubated with captured EVs for 0.5 h at room temperature, followed by magnetic separation; 1 μM of the NA probe and 0.1 U of the DSN enzyme in a 30 μL reaction with 5 mM Mg^{2+} were added into the system and incubated at 60 °C for 2 h. The fluorescent signal was measured by a fluorescence spectrophotometer. The linear relationship was explored by incubation with RNA and EVs of different concentrations. Plasma EVs were isolated and detected by the AbMB−biChol platform. For plasma detection, 100 μL of plasma was incubated with 20 μL of AbMBs and detected by the biChol platform as described before.

Amplification Refractory Mutation System PCR (ARMS-PCR). The mutated KRAS was detected by amplification refractory mutation system PCR (ARMS-PCR). Total nucleic acid was extracted by the cell-free nucleic extraction kit and cDNA was synthesized by the following methods: 4 μL of 5 × RT buffer, 1 μL of the dNTP mix (10 nM), 1 μL of the RNA inhibitor (40 U/μL), 1 μL of the RT primer (20 nM), 1 μL of reverse transcriptase (100 U/μL), total RNA extracted from real samples, and DEPC-treated water were mixed to a final volume of 20 μL. The prime for ARMS-PCR was designed with two allelic mismatches compared to the wild type, and one allelic mismatch compared to the mutated type. The ARMS-PCR was conducted under the following conditions: 5 μL of 2 × AceTaq master mix, 0.2 μL of the forward ARMS primer (10 μM), 0.2 μL of the reverse primer (10 μM), 0.4 μL of the Taqman probe (10 μM), 2 μL of the RT product, and DEPC-treated water were mixed to a final volume of 10 μL. The qRT-PCR process was conducted under the following conditions: 95 °C for 5 min, 40 cycles of 95 °C for 10 s, and 55 °C for 30 s. The fluorescence signal was detected at 55 °C. The sequences of primers are listed in Table S2.

Interaction and Affinity Determination between the Cholesterol-Modified Duplex and the Membrane. The quartz crystal microbalance (QCM) method was utilized to explore the affinity between cholesterol and the bilayer membrane. First of all, the PANC-1 cell was cultured and fixed on the COP-1 chip of the Attana Cell 200 with a 4% formaldehyde solution for 15 min. Then, the cholesterol-modified duplex (50 nM) at a flow rate of 250 μL/min was injected and the real-time change of vibration frequency (Δf) was recorded. Once injection was stopped, the change of the vibration frequency curve was used to evaluate the combination force between cholesterol and the membrane. The larger absolute value of the slope represented the weaker or nonspecific combination.

Protein Extraction and Western Blot Analysis. Captured EVs were mixed with loading buffer and heated to 100 °C for 15 min for denaturation, and then western blot analysis was carried out on 8% SDS-PAGE according to the protocol and electrotransferred onto nitrocellulose filters. After blocking in TBS with 0.1% Tween 20 (TBST) and 5% skim milk for 1 h at the same temperature, the membranes were incubated with the specific primary antibody in TBST containing 5% BSA at 4 °C overnight. The HRP-labeled secondary antibody was added, washed 3 times with TBST, and incubated for 1 h at room temperature. Then, the developing agent was added dropwise onto the nitrocellulose filters, and bands were scanned by Quantity One Imaging Software from Bio-Rad.

Enzyme-Linked Immunosorbent Assay (ELISA). EGFR, EpCAM, GPC1, and EphA2 protein expressions were determined by the ELISA kit according to the protocol.

https://doi.org/10.1021/acs.analchem.1c01712
Anal. Chem. 2021, 93, 9860−9868

Briefly, 0.1 mL of the diluted antibody (1 g/mL) was added into the reaction hole and placed at 4 °C overnight. The diluted sample (0.05 mL) to be tested and 0.05 mL of the fresh diluted enzyme standard antibody were added into the hole and incubated at 37 °C for 1 h successively. Then, 0.1 mL of the 3,3′,5,5′-tetramethylbenzidine (TMB) substrate solution was prepared, added in each reaction hole, and incubated at 37 °C for 10−30 min. Sulfuric acid (2 M, 0.05 mL) was added to stop the reaction, and the OD value was measured using a microplate reader at 450 nm.

Statistical Analysis. Data were presented as mean ± standard deviation (SD). The statistical significance between different groups was calculated via *t*-test analysis using GraphPad Prism 8.2.

RESULTS AND DISCUSSION

Proof-of-Principle Validation of EV Capture by the AbMB Platform. The magnetic isolation of the prepared immunobeads accompanied by target EVs was the primary step of the whole process and was characterized by various methods. First, transmission electron microscopy (TEM) and scanning electron microscopy (SEM) were employed to characterize the AbMB interface when harvesting PANC-1 EVs in phosphate-buffered saline (PBS), which was collected by ultracentrifugation and is characterized in Figure S1. As shown in Figure 1a, representative transmission electron microscopy (TEM) and scanning electron microscopy (SEM) images revealed the harvested EVs on EGFR-AbMB, and the inset images indicated that the captured EVs exhibit spherical or cup-shaped morphologies. No EVs were observed on IgG-conjugated protein A/G beads by either TEM or SEM, reflecting that the nonspecific adsorption of the MBs was ignorable (Figure S2). The tetraspanins CD63, CD9, and CD81 were expressed in both the cell lysate and the MB-bound precipitate, while the expression of the EV-irrelevant protein calnexin was negligible in the precipitate, indicating that the EVs were precisely captured (Figure 1b). In addition, PANC-1-derived EVs were first labeled with the fluorescent dye PKH 67 so that they could be directly tracked by the fluorescence microscope. The micrographs in Figure 1c exhibited conspicuous EV signals around AbMBs, evidencing that the EVs were successfully captured.

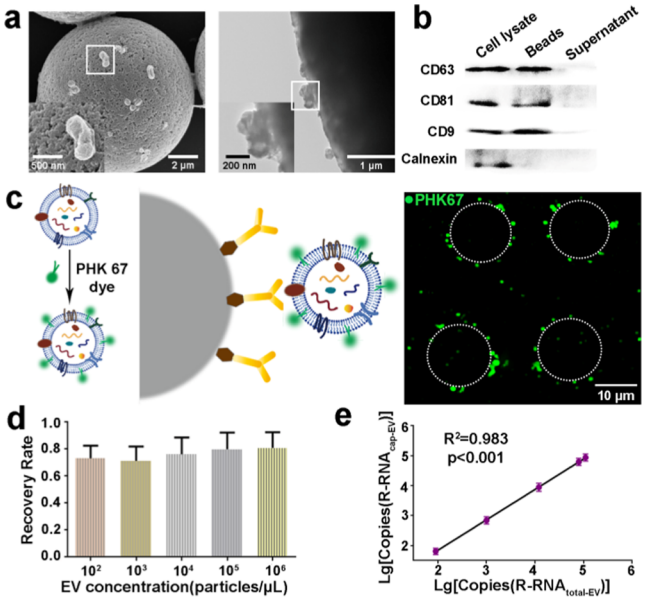

Figure 1. Characterization and validation of EV capture efficiency via AbMBs. (a) TEM and SEM images of AbMBs with captured EVs. (b) Western blot analysis of the EV protein biomarker expression in the corresponding cell lysate, MBs, and supernatant. (c) Schematic illustration of AbMB-captured EVs incubated with the EV membrane dye PHK 67 and fluorescence of the captured EVs. The white dotted circles represented MBs. (d) The capture rate of EVs with different concentrations via AbMBs. (e) The capture rate determined by the random RNA (R-RNA) recovery rate before and after AbMB separation.

For the accurate evaluation of the performance of AbMBs, RNA with random sequence (R-RNA) was used as a tag for PANC-1 EVs, which was designed to be sorted into EVs with a specific 3′-GGAG motif[34] and transfected into cells in advance. After separation via AbMBs, R-RNA was extracted and determined by RT-qPCR. The presence of the R-RNA tag allowed reliable quantification of PANC-1-derived EVs. The recovery rate of AbMBs under a given condition was defined by comparing the R-RNA copies in total EVs (total-EV) and captured EVs (cap-EV). The average capture rate of the AbMB platform was approximately 80% (Figure 1d). Then, we confirmed the accuracy of the capture rate (R^2 = 0.9832) using various EV concentrations containing 90−110 000 copies of R-RNA transcripts per 100 μL volume (Figure 1e). In addition, the optimized conditions were further explored as described in Figures S3 and S4. The antibody combination was first verified by Coomassie blue staining and the uncombined antibody in the supernatant was determined by UV absorbance for the confirmation of the best ratio (20 μL of MBs: 4 μg of the antibody) and incubation time (1 h). Then, the optimum incubation condition of EVs was determined directly profited from the R-RNA tag in EVs. The best incubation time was 1 h. The incubation temperature (4 °C or room temperature) and order of incubation (antibodies incubated with EVs and then beads or antibodies incubated with beads and then EVs) did not significantly affect the EV capture efficiency, as verified by the approximative recovery rate of the EVs.

Verification and Quantification of the Amplification System. In addition to efficient capture, ultrasensitivity is a prerequisite for samples with limited volumes and low EV abundance. In the cholesterol-mediated anchor strategy, the EV signal was successfully transmitted to the nucleic acid signal, laying the foundation for a DSN-assisted signal amplification cycle (Figure 2a). The DNA probe modified with FAM (fluorescence group) and BHQ-1(quenching group) on the separated end of the sequence was complementary to the RNA of the cholesterol-labeled RNA−DNA duplex. Owing to the specific cleavage ability of DSN, the DNA of the RNA−DNA duplex was selectively digested by DSN, subsequently leading to the fluorescence signal being turned on (Figure S5). The RNA signal amplification process and fluorescence (FL) intensity of target RNA at different concentrations are illustrated in Figure 2b. After calibrating the FL intensity to that of the control, the FL changes exhibited a linear dependence on the logarithm (lg) of duplex concentrations (ranging from 10 pM to 10 nM), and the correlation equation $(F/F0 - 1) = 100.2x - 85.45 \lg C$ (RNA) (R^2 = 0.990) was obtained, where $F0$ and F represented the FAM fluorescence signal in the absence and presence of target RNA, respectively (Figure 2c). Similarly, after the cholesterol-modified RNA−DNA duplex was inserted into the EV membrane, a linear relationship was observed between the

https://doi.org/10.1021/acs.analchem.1c01712
Anal. Chem. 2021, 93, 9860−9868

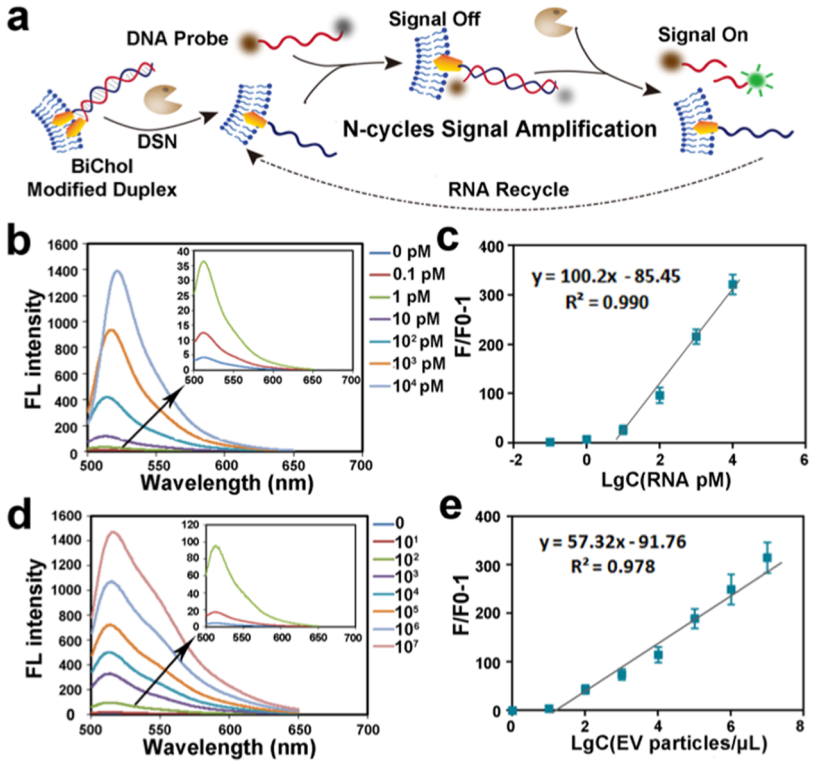

Figure 2. Amplified quantification of RNA in the RNA−DNA duplex and EVs. (a) Schematic illustration of DSN-based amplified detection cycles. Fluorescence emission spectra (excitation at 488 nm and emission at 520 nm) upon addition of the (b) RNA−DNA duplex and the (d) EVs at different concentrations. Inset: fluorescence responses to the duplex or EVs at low concentrations. The scatter plot of $(F/F0 - 1)$ as a function of the concentrations of (c) the RNA−DNA duplex and (e) EVs, where $F0$ and F were the FAM fluorescence signals in the absence and presence of RNA−DNA or EVs, respectively.

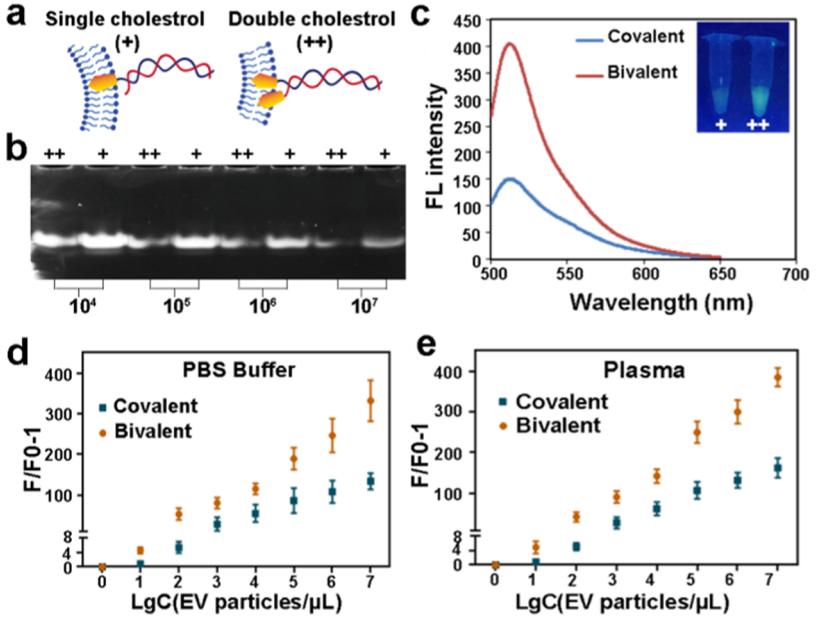

Figure 3. Membrane affinity comparison between covalent and bivalent cholesterol-modified duplexes. (a) Schematic illustration of the anchor pattern of single and double cholesterol-modified duplexes into the phospholipid bilayer. (b) PAGE gel electrophoresis analysis of the uncombined duplex in the supernatant after incubation with EVs of different concentrations (10^4, 10^5, 10^6, and 10^7 particles/μL). ++: bivalent duplex modified with double cholesterol and +: covalent duplex modified with single cholesterol. (c) Fluorescence emission spectra of the covalent and bivalent cholesterol-modified duplex detection platform with the same concentration of EVs. Inset: fluorescence images of corresponding systems. Fluorescence responses to EVs with different concentrations diluted in the (d) PBS buffer and (e) EV-free plasma, where $F0$ and F were the FAM fluorescence signals in the absence and the presence of EVs, respectively.

change in FL intensity and the EV concentrations (Figure 2d), with the equation $(F/F0 - 1) = 57.32x - 91.76 \lg C$ (EV) (R^2 = 0.978, Figure 2e). Moreover, the limit of detection (LOD) indicated in Figure 2e was approximately 10 particles/μL

https://doi.org/10.1021/acs.analchem.1c01712
Anal. Chem. 2021, 93, 9860−9868

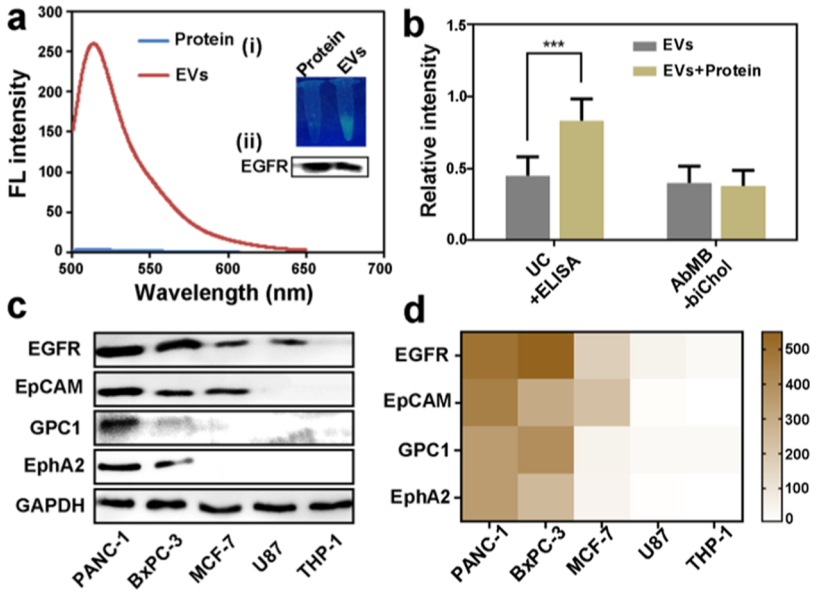

Figure 4. Specificity of EV detection via the AbMB−biChol platform. (a) Fluorescence emission spectrum obtained for the AbMB−biChol platform in the detection of the total protein and EVs from PANC-1 cells. Inset: (i) fluorescence image corresponding to the fluorescence emission spectrum and (ii) EGFR expression level in the total protein and EVs. (b) EV quantification determined by the UC-ELISA assay and AbMB−biChol in the EVs and EV−protein mixtures. (c) Expression of membrane proteins EGFR, EpCAM, GPC1, and EphA2 in different cell lines determined by western blot analysis. (d) Expression of the EVs in different cell lines as determined by the AbMB−biChol platform modified with corresponding antibodies.

(Blank + 3SD), which was superior to that of most previously reported methods (Table S3). The described amplification platform possesses favorable EV detection accuracy and sensitivity and can be applied to limited sample volumes for the detection of EVs.

Optimization of the Cholesterol-Based RNA Anchoring Strategy. The cholesterol-based anchor of DNA or RNA has been widely reported in biomedical applications, and the cholesterol anchoring efficiency was essential to the sensitivity of the described method and had great relevance to the amount of the RNA−DNA duplex anchored. However, the covalent anchoring of cholesterol was relatively weak,[25] resulting in insufficient cholesterol binding and signal transfer efficiency. To further improve the strength of cholesterol-based coupling to the lipid membrane, a bivalent coupling of the RNA−DNA duplex was developed by hybridizing equivalent 5′-end cholesterol-modified RNA and 3′-end cholesterol-modified DNA. A duplex with single-strand cholesterol modification (covalent cholesterol) was investigated for comparison, as illustrated in Figure 3a. After incubation with different amounts of EVs and AbMB-captured EVs for the same amount of time, the covalent cholesterol-modified duplex was observed at a higher concentration in the supernatant than the bivalent cholesterol duplex, indicating that less duplex was inserted into the EV membrane (Figure 3b). Similar results were observed in the fluorescence signal in the DSN-assisted amplification system, as exhibited in Figure 3c. The responsive fluorescence signal emerged when target EVs and DSN existed (Figure S6). The interaction between the cholesterol-modified duplex and the EV membrane was further explored with an Attana Cell 200 system, which is a quartz crystal microbalance (QCM) system for the study of the interaction between membranes and the bivalent cholesterol-modified duplex. The cell membranes were first fixed on chips, and then the covalent or bivalent cholesterol-modified duplex was injected. During the dissociation period, the change in frequency ($-\Delta f$) decreased more obviously in the covalent cholesterol system, indicating that a stronger binding force was achieved in the bivalent cholesterol system (Figure S7). To verify the behavior of the bivalent cholesterol-modified duplex in different media, EV detection was conducted in PBS buffer and EV-free human plasma. In all of the tested EV solutions, the fluorescence signals increased corresponding to EV concentrations, as exhibited in Figure 3d,e. Typically, the signal intensity in the bivalent cholesterol system was higher than that in the covalent cholesterol system at the same EV concentration, confirming the favorable sensitivity and potency of the bivalent cholesterol modification strategy.

Specific and Selective Detection of EVs via the AbMB−biChol Platform. To determine the detection specificity of the AbMB−biChol platform, the EV discrimination capacity from the protein was investigated. First of all, the free total protein was extracted from PANC-1 cells using the protein extraction kit, and EVs were collected by ultracentrifugation. As shown in Figure 4a, when the free protein without any lipid component incubated with the AbMB−biChol platform, no fluorescence signal was observed, indicating the incapable binding between the protein and the cholesterol-modified duplex, despite the fact that target protein (EGFR) expressions were detected in both the cell lysate and EVs by western blot. Then, we divided EVs into two parts, and one was introduced with the free total protein (EV−protein mixture). To demonstrate the EV specificity and compared it with the proposed AbMB−biChol platform, ultracentrifugation (UC) together with the ELISA kit was utilized to describe the EGFR expression of individual EVs and EV−protein mixtures. An obvious protein increase was observed in the UC + ELISA group, indicating that some free protein was settled by ultracentrifugation. However, no big difference was observed in the AbMB−biChol platform. The free protein was unable to interfere with EVs in the AbMB−biChol detection process. The UC + ELISA assay for EV quantification was affected by

https://doi.org/10.1021/acs.analchem.1c01712
Anal. Chem. 2021, 93, 9860−9868

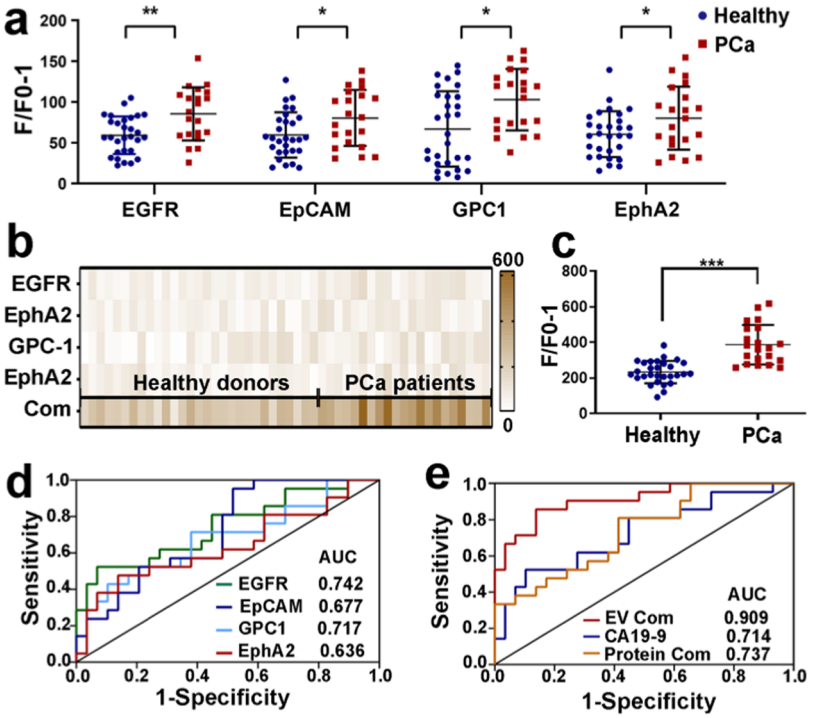

Figure 5. Differentiation of PCa patients and healthy donors based on plasma EVs detected by the AbMB−biChol platform. (a) Scatter plots of the fluorescence signals obtained for PCa patients (n = 21) and healthy donors (n = 29) via the AbMB−biChol platform modified with EGFR, EpCAM, GPC1, and EphA2. (b) Heatmap of the fluorescence signals obtained for PCa patients and healthy donors. (c) Scatter plot of the fluorescence signals after combination. (d) Receiver operating characteristic (ROC) curves of the separated antibody-modified platform. (e) Comparison of the ROC curves of the EV combination, CA19-9, and protein combination. Com referred to the unweighted combination. Statistical significance was calculated via t-test analysis. *P < 0.05 and **P < 0.01.

the protein to a great extent, while the AbMB−biChol platform was able to recognize the EVs and exclude any protein disturbances, with no significant signal difference before and after protein addition. The AbMB−biChol platform ensured the EV-specific identification in complex samples (Figure 4b).

Furthermore, benefitting from the affinity of the antibodies, the AbMB−biChol platform was used to identify different cell-derived EVs with unique protein expression levels. Four membrane proteins (EGFR, EpCAM, GPC1, and EphA2) were selected as biomarkers for PCa cell lines, and the corresponding expression levels in different cells were determined by western blot analysis. As shown in Figure 4c, the PCa cell lines PANC-1 and BxPC-3 exhibited higher protein expression levels for the four proteins investigated than other cells, supporting that the selected biomarkers were available for PCa. Consistent with the cell expression profile, the EVs derived from different cell lines exhibited similar characteristics, as determined by the AbMB−biChol platform (Figure 4d), revealing the practicability of the proposed EV identification platform for PCa discrimination.

Clinical Application of the AbMB−biChol Platform. Considering the liquid biopsy features of EVs, we further explored the clinical utility of the AbMB−biChol platform in EV-based pancreatic cancer detection. First of all, 21 PCa patients and 29 healthy donors were recruited as a panel for the detection of EV via four separate AbMB−biChol (modified with EGFR, EpCAM, GPC1, and EphA2 antibodies). Differences existed in all four groups, as displayed in Figure 5a. Furthermore, the PCa diagnostic efficacy was greatly enhanced in the unweighted combination platform employing 4 equiv of AbMB−biChols, as shown in the heatmap and scatter plot in Figure 5b,c. The combination platform (AUC: 0.909) outperformed the separated platform conjugated with a single antibody (Figure 5d) and the widely used serum biomarker CA19-9 (AUC: 0.714) for PCa diagnosis (Figure 5e), as displayed in their ROC curves. Notably, the discrimination effectiveness arose from the difference in the abundance of EVs rather than four PCa-related proteins. No significant differences were observed in the plasma protein expression levels of EGFR, EpCAM, GPC1, and EphA2 between PCa patients and healthy donors, which was determined by ELISA (Figure S8), and no diagnostic improvement was achieved in the unweighted combination of four protein markers (AUC: 0.737) compared with CA19-9 (Figure 5e), revealing that EVs have diagnostic advantages over proteins in plasma samples.

Since KRAS mutation is widely reported in pancreatic cancer,[2] it was selected as a benchmark for PCa-derived EVs in this study. The expression levels of the most common KRAS DNA mutations (G12D, G12V, and G12R) in the EVs captured by the AbMB platform were significantly higher in PCa patients than in healthy donors. Mutation rates in the captured EVs were 79% (G12D), 62% (G12V), and 17.2% (G12R) for PCa patients and 0% (G12D, G12V, and G12R) for healthy donors (Figure S9). These results indicated a strong correlation between captured EVs and PCa, confirming the clinical application potential of the proposed EV detection system for PCa auxiliary diagnosis.

CONCLUSIONS

In summary, we presented an EV differentiation platform with high specificity and sensitivity. We introduced bivalent

https://doi.org/10.1021/acs.analchem.1c01712
Anal. Chem. 2021, 93, 9860−9868

cholesterol-modified RNA−DNA duplexes and a signal amplification strategy assisted by the selective cleavage enzyme DSN to convert an EV signal into an amplified RNA signal. The bivalent cholesterol strategy improved the anchoring efficiency of the duplex, allowing it to irreversibly bind to the EV membrane. Consequently, the antibody-modified magnetic beads along with the bivalent cholesterol-based amplification detection system enabled profound EV capture and detection efficiency, achieving a LOD of 10 particles/μL, which is competitive with current EV analysis methods. Moreover, the AbMB−biChol system allowed differentiation of EVs originated from various cancer cells, realizing cell-traceable EV identification. After inosculated with antibodies against PCa-related biomarkers, the proposed biosensor exhibited great promise for PCa-related EV identification and PCa diagnosis, demonstrating superior characteristics to CA19-9 and four PCa-related protein combination analysis, embracing great potential in clinical applications.

■ ASSOCIATED CONTENT

Supporting Information

The Supporting Information is available free of charge at https://pubs.acs.org/doi/10.1021/acs.analchem.1c01712.

Clinical information of PCa cohort; sequences of oligonucleotides used in this work; characterization of EVs and magnetic beads; assay optimization and performance investigation; protein expressions levels and KRAS mutation determination; and comparison of EV detection assays (PDF)

■ AUTHOR INFORMATION

Corresponding Authors

Yi Ma − *Department of Biomedical Engineering, School of Engineering, China Pharmaceutical University, Nanjing 211198, China*; Email: yima@163.com

Yueqing Gu − *Department of Biomedical Engineering, School of Engineering, China Pharmaceutical University, Nanjing 211198, China*; orcid.org/0000-0003-1315-4618; Email: guengineering@cpu.edu.cn

Authors

Ping Li − *Department of Biomedical Engineering, School of Engineering, China Pharmaceutical University, Nanjing 211198, China*

Jie Wang − *The Affiliated Hospital of Qingdao University, Qingdao University, Qingdao 266071, China*

Mengqiu Gao − *Department of Biomedical Engineering, School of Engineering, China Pharmaceutical University, Nanjing 211198, China*

Jue Wang − *Department of Biomedical Engineering, School of Engineering, China Pharmaceutical University, Nanjing 211198, China*

Complete contact information is available at: https://pubs.acs.org/10.1021/acs.analchem.1c01712

Author Contributions

P.L. and J.W. contributed equally. All authors contributed to the conception of the experiments and discussion of the results and contributed to writing the manuscript. All authors have given approval to the final version of the manuscript.

Notes

The authors declare no competing financial interest.

■ ACKNOWLEDGMENTS

The work was primarily supported by the National Natural Science Foundation of China (NSFC 91859204, 81729002, and 81727804), the Open Project of State Key Laboratory of Natural Medicines (SKLNMZZCX201819), and the "Double-First Class" Developing Project of China Pharmaceutical University (CPU2018CY24). The authors also thank Jiangsu Cancer Hospital for providing plasma samples.

■ REFERENCES

(1) Quante, A. S.; Ming, C.; Rottmann, M.; Engel, J.; Boeck, S.; Heinemann, V.; Westphalen, C. B.; Strauch, K. *Cancer Med.* **2016**, *5*, 2649−2656.

(2) Kruger, S.; Heinemann, V.; Ross, C.; Diehl, F.; Nagel, D.; Ormanns, S.; Liebmann, S.; Prinz-Bravin, I.; Westphalen, C. B.; Haas, M.; Jung, A.; Kirchner, T.; von Bergwelt-Baildon, M.; Boeck, S.; Holdenrieder, S. *Ann. Oncol.* **2018**, *29*, 2348−2355.

(3) Raposo, G.; Stoorvogel, W. *J. Cell Biol.* **2013**, *200*, 373−383.

(4) Raposo, G.; Stahl, P. D. *Nat. Rev. Mol. Cell Biol.* **2019**, *20*, 509−510.

(5) Rahbarghazi, R.; Jabbari, N.; Sani, N. A.; Asghari, R.; Salimi, L.; Kalashani, S. A.; Feghhi, M.; Etemadi, T.; Akbariazar, E.; Mahmoudi, M.; Rezaie, J. *Cell Commun. Signaling* **2019**, *17*, No. 73.

(6) Lane, R. E.; Korbie, D.; Hill, M. M.; Trau, M. *Clin. Transl. Med.* **2018**, *7*, No. 14.

(7) van der Pol, E.; Boing, A. N.; Harrison, P.; Sturk, A.; Nieuwland, R. *Pharmacol. Rev.* **2012**, *64*, 676−705.

(8) Lewis, J. M.; Vyas, A. D.; Qiu, Y.; Messer, K. S.; White, R.; Heller, M. J. *ACS Nano* **2018**, *12*, 3311−3320.

(9) Boukouris, S.; Mathivanan, S. *Proteomics: Clin. Appl.* **2015**, *9*, 358−367.

(10) Fais, S.; O'Driscoll, L.; Borras, F. E.; Buzas, E.; Camussi, G.; Cappello, F.; Carvalho, J.; da Silva, A. C.; Del Portillo, H.; El Andaloussi, S.; Trcek, T. F.; Furlan, R.; Hendrix, A.; Gursel, I.; Kralj-Iglic, V.; Kaeffer, B.; Kosanovic, M.; Lekka, M. E.; Lipps, G.; Logozzi, M.; Marcilla, A.; Sammar, M.; Llorente, A.; Nazarenko, I.; Oliveira, C.; Pocsfalvi, G.; Rajendran, L.; Raposo, G.; Rohde, E.; Siljander, P.; van Niel, G.; Vasconcelos, M. H.; Yanez-Mo, M.; Yliperttula, M. L.; Zarovni, N.; Zavec, A. B.; Giebel, B. *ACS Nano* **2016**, *10*, 3886−3899.

(11) Shao, H. L.; Chung, J.; Balaj, L.; Charest, A.; Bigner, D. D.; Carter, B. S.; Hochberg, F. H.; Breakefield, X. O.; Weissleder, R.; Lee, H. *Nat. Med.* **2012**, *18*, 1835−1840.

(12) Al-Nedawi, K.; Meehan, B.; Micallef, J.; Lhotak, V.; May, L.; Guha, A.; Rak, J. *Nat. Cell Biol.* **2008**, *10*, 619−624.

(13) Melo, S. A.; Luecke, L. B.; Kahlert, C.; Fernandez, A. F.; Gammon, S. T.; Kaye, J.; LeBleu, V. S.; Mittendorf, E. A.; Weitz, J.; Rahbari, N.; Reissfelder, C.; Pilarsky, C.; Fraga, M. F.; Piwnica-Worms, D.; Kalluri, R. *Nature* **2015**, *523*, 177−182.

(14) Liang, K.; Liu, F.; Fan, J.; Sun, D. L.; Liu, C.; Lyon, C. J.; Bernard, D. W.; Li, Y.; Yokoi, K.; Katz, M. H.; Koay, E. J.; Zhao, Z.; Hu, Y. *Nat. Biomed. Eng.* **2017**, *1*, No. 0021.

(15) Li, W. Z.; Shao, B.; Liu, C. L.; Wang, H. Y.; Zheng, W. S.; Kong, W. Y.; Liu, X. R.; Xu, G. B.; Wang, C.; Li, H. P.; Zhu, L.; Yang, Y. L. *Small Methods* **2018**, *2*, No. 1800122.

(16) Rayyan, M.; Zheutlin, A.; Byrd, J. B. *J. Extracell. Vesicles* **2018**, *7*, No. 1535744.

(17) Wang, J.; Wuethrich, A.; Ibn Sina, A. A.; Lane, R. E.; Lin, L. L.; Wang, Y. L.; Cebon, J.; Behren, A.; Trau, M. *Sci. Adv.* **2020**, *6*, No. eaax3223.

(18) Shao, H.; Im, H.; Castro, C. M.; Breakefield, X.; Weissleder, R.; Lee, H. *Chem. Rev.* **2018**, *118*, 1917−1950.

(19) Chen, X. S.; Lan, J. M.; Liu, Y. X.; Li, L.; Yan, L.; Xia, Y. K.; Wu, F.; Li, C. Y.; Li, S. R.; Chen, J. H. *Biosens. Bioelectron.* **2018**, *102*, 582−588.

(20) Wu, L.; Wang, Y.; Xu, X.; Liu, Y.; Lin, B.; Zhang, M.; Zhang, J.; Wan, S.; Yang, C.; Tan, W. Aptamer-Based Detection of Circulating Targets for Precision Medicine *Chem. Rev.* 2021, DOI: 10.1021/acs.chemrev.0c01140.

(21) Wei, P.; Wu, F.; Kang, B.; Sun, X.; Heskia, F.; Pachot, A.; Liang, J.; Li, D. *J. Extracell. Vesicles* **2020**, *9*, No. 1809765.
(22) Xu, L.; Chopdat, R.; Li, D.; Al-Jamal, K. T. *Biosens. Bioelectron.* **2020**, *169*, No. 112576.
(23) Hoshino, A.; Kim, H. S.; Bojmar, L.; Gyan, K. E.; Cioffi, M.; Hernandez, J.; Zambirinis, C. P.; Rodrigues, G.; Molina, H.; Heissel, S.; Mark, M. T.; Steiner, L.; Benito-Martin, A.; Lucotti, S.; Di Giannatale, A.; Offer, K.; Nakajima, M.; Williams, C.; Nogues, L.; Pelissier Vatter, F. A.; Hashimoto, A.; Davies, A. E.; Freitas, D.; Kenific, C. M.; Ararso, Y.; Buehring, W.; Lauritzen, P.; Ogitani, Y.; Sugiura, K.; Takahashi, N.; Aleckovic, M.; Bailey, K. A.; Jolissant, J. S.; Wang, H.; Harris, A.; Schaeffer, L. M.; Garcia-Santos, G.; Posner, Z.; Balachandran, V. P.; Khakoo, Y.; Raju, G. P.; Scherz, A.; Sagi, I.; Scherz-Shouval, R.; Yarden, Y.; Oren, M.; Malladi, M.; Petriccione, M.; De Braganca, K. C.; Donzelli, M.; Fischer, C.; Vitolano, S.; Wright, G. P.; Ganshaw, L.; Marrano, M.; Ahmed, A.; DeStefano, J.; Danzer, E.; Roehrl, M. H. A.; Lacayo, N. J.; Vincent, T. C.; Weiser, M. R.; Brady, M. S.; Meyers, P. A.; Wexler, L. H.; Ambati, S. R.; Chou, A. J.; Slotkin, E. K.; Modak, S.; Roberts, S. S.; Basu, E. M.; Diolaiti, D.; Krantz, B. A.; Cardoso, F.; Simpson, A. L.; Berger, M.; Rudin, C. M.; Simeone, D. M.; Jain, M.; Ghajar, C. M.; Batra, S. K.; Stanger, B. Z.; Bui, J.; Brown, K. A.; Rajasekhar, V. K.; Healey, J. H.; de Sousa, M.; Kramer, K.; Sheth, S.; Baisch, J.; Pascual, V.; Heaton, T. E.; La Quaglia, M. P.; Pisapia, D. J.; Schwartz, R.; Zhang, H.; Liu, Y.; Shukla, A.; Blavier, L.; DeClerck, Y. A.; LaBarge, M.; Bissell, M. J.; Caffrey, T. C.; Grandgenett, P. M.; Hollingsworth, M. A.; Bromberg, J.; Costa-Silva, B.; Peinado, H.; Kang, Y.; Garcia, B. A.; O'Reilly, E. M.; Kelsen, D.; Trippett, T. M.; Jones, D. R.; Matei, I. R.; Jarnagin, W. R.; Lyden, D. *Cell* **2020**, *182*, 1044−1061.
(24) Rodrigues, M.; Richards, N.; Ning, B.; Lyon, C. J.; Hu, T. Y. *Nano Lett.* **2019**, *19*, 7623−7631.
(25) Pfeiffer, I.; Hook, F. *J. Am. Chem. Soc.* **2004**, *126*, 10224−10225.
(26) Ferrer, J. R.; Sinegra, A. J.; Ivancic, D.; Yeap, X. Y.; Qiu, L.; Wang, J. J.; Zhang, Z. J.; Wertheim, J. A.; Mirkin, C. A. *ACS Nano* **2020**, *14*, 1682−1693.
(27) He, F.; Liu, H.; Guo, X. G.; Yin, B. C.; Ye, B. C. *Anal. Chem.* **2017**, *89*, 12968−12975.
(28) He, F.; Wang, J.; Yin, B. C.; Ye, B. C. *Anal. Chem.* **2018**, *90*, 8072−8079.
(29) Pan, Y. H.; Wang, L.; Deng, Y.; Wang, M.; Peng, Y.; Yang, J.; Li, G. *Chem. Commun.* **2020**, *56*, 13768−13771.
(30) Lagos-Quintana, M.; Rauhut, R.; Lendeckel, W.; Tuschl, T. *Science* **2001**, *294*, 853−858.
(31) Yin, B. C.; Liu, Y. Q.; Ye, B. C. *J. Am. Chem. Soc.* **2012**, *134*, 5064−5067.
(32) Clotilde, T.; Sebastian, A.; Graca, R.; Aled, C. *Curr. Protoc. Cell Biol.* **2006**, *30*, 3−22.
(33) Sun, N.; Lee, Y. T.; Zhang, R. Y.; Kao, R.; Teng, P. C.; Yang, Y.; Yang, P.; Wang, J. J.; Smalley, M.; Chen, P. J.; Kim, M.; Chou, S. J.; Bao, L.; Wang, J.; Zhang, X.; Qi, D.; Palomique, J.; Nissen, N.; Han, S. B.; Sadeghi, S.; Finn, R. S.; Saab, S.; Busuttil, R. W.; Markovic, D.; Elashoff, D.; Yu, H. H.; Li, H.; Heaney, A. P.; Posadas, E.; You, S.; Yang, J. D.; Pei, R.; Agopian, V. G.; Tseng, H. R.; Zhu, Y. *Nat. Commun.* **2020**, *11*, No. 4489.
(34) Villarroya-Beltri, C.; Gutierrez-Vazquez, C.; Sanchez-Cabo, F.; Perez-Hernandez, D.; Vazquez, J.; Martin-Cofreces, N.; Martinez-Herrera, D. J.; Pascual-Montano, A.; Mittelbrunn, M.; Sanchez-Madrid, F. *Nat. Commun.* **2013**, *4*, No. 2980.

https://doi.org/10.1021/acs.analchem.1c01712
Anal. Chem. 2021, 93, 9860−9868